ARTICLE OPEN

Check for updates

Protective coatings for ceramic artefacts exposed to UV ageing

Andrei V. Oancea[1], George Bodi[2], Adrian Cernescu[3], Iuliana Spiridon[1], Alina Nicolescu[1], Mioara Drobota[1], Corneliu Cotofana[1], Bogdan C. Simionescu[1,4] and Mihaela Olaru[1]✉

The commercial acrylic copolymer Paraloid B72 (PB72) and a synthesized nanostructured material (AMF) bearing silsesquioxane, methacrylate and fluorine units were analyzed to assess their performances as protective coatings for the conservation of Neolithic Cucuteni ceramic pottery when submitted to UV ageing. In the context of comparative evaluation of the protective efficiency, the present paper reports the use of a functional coating that operates *via* specific photochemical transformations at the coating-air interface as a UV resistant protection coating for cultural heritage artefacts. The main factors that influenced the photo-degradation behavior of the polymeric materials included their structure, the properties at the polymer/air interfaces, and the preferential orientation of functional groups at the surface of the polymeric coatings.

npj Materials Degradation (2023)7:21 ; https://doi.org/10.1038/s41529-023-00343-8

INTRODUCTION

Ceramic artifacts survive for thousands of years and provide information regarding the culture and technology of their manufacturers. Ceramics are usually subjected to physical or chemical degradation, and external factors such as water, soluble salts, impact and abrasions, frost and mold growth can dramatically affect their aspect and properties. Until recently, the conservation of ceramics relied on products designed for stone and glass and, due to commercial reasons, research into conservation treatments for ceramics is scarce[1,2] and limited in scope.

Acrylic polymers and copolymers are extensively used as protective coatings for cultural heritage due to their good film forming properties, adhesion, non-wettability and chemical inertness. However, the limited environmental stability of most acrylic-based compounds makes them inappropriate to adequately accomplish the long term requirements of efficient protective coatings, i.e., water repellency and vapour permeability, transparency, durability, negligible influence on the substrates, and reversibility or easy removal[3]. Water repellent nanostructured coatings for monumental stones with silsesquioxane and methacrylate units were previously reported to present high durability against salt mist and SO_2 action in humid environment[4–7]. The introduction of fluorine atoms inside polymeric networks improved chemical, thermal and photochemical stability and hydrophobicity[8]. As regards poly(meth)acrylates bearing semi-fluorinated side chains, the appearance of highly ordered surfaces with CF_3 groups disposed on the top layer due to an internal microphase separation was observed[9]. Poly(fluoromethacrylate)s present unique characteristics including reduced friction coefficients, low surface energies, non-adhesive nature, water and oil repellency and solid state assembly into smectic layers, making them suitable as chemical resistant antifouling coatings[10].

UV radiation is a major degradation agent of protective coatings for cultural heritage objects. The natural ageing of protective coatings influences their macroscopic characteristics due to alteration of optical properties, i.e., color changes, transparency loss, changes in solubility, brittleness, loss of material strength, cracking and peeling due to chemical modifications including crosslinking reactions. The degradation of the coatings allows the penetration of soluble salts that, upon crystallization, induce stress and damage items. In order to improve the durability of protective coatings, several types of organic and inorganic UV absorbers and light stabilizers have been added to polymeric coatings[11,12]. UV absorbers can react with radicals formed during photo-degradation and preventing chain scission or cleavage of the side groups, while light stabilizers can absorb certain UV radiations and reduce discoloration caused by weathering. These compounds present several drawbacks with no single UV absorber able to induce the complete absorption of UV light and transparency of visible light[13] and more stable inorganic nanoparticles agregating[14]. Light stabilizers are expensive and effective only in short-term exposures. UV-resistant polymeric protective coatings that do not rely on UV absorbers or light stabilizers would have many practical applications.

Functional coatings rely on a specific chemical, physical, thermal or mechanical property or a combination thereof. Chemically active functional coatings present unique properties either in bulk or at the coating-substrate or coating-air interfaces. Increasingly studied are surface functional coatings that operate *via* specific chemical transformations onto or near the film/air interface leading to low free energy surface, improved chemical, thermal and light resistance or outstanding mechanical properties[15]. The outer coating interface is formed due to photo- or biochemical reactions between environmental compounds or an external energy source (sunlight, heat) and the components coming from the bulk are oriented towards the coating interface. Such surface functional coatings have been previously reported for pollutant destructing, self-cleaning, antifouling and antibacterial coatings[15].

The present article describes a comparative evaluation of the protective efficiency against UV irradiation of two polymeric water repellent coatings that do not comprise any UV stabilizers or fillers for nine ceramic samples of Neolithic Cucuteni pottery. The two coatings were the commercial product Paraloid B72 (PB72—p(MA-EMA), methylacrylate-ethylmethacrylate copolymer, 30/70 w/w%) and a synthesized nanostructured material (AMF) bearing

[1]"Petru Poni" Institute of Macromolecular Chemistry, 41A Gr. Ghica Voda Alley, 700487 Iasi, Romania. [2]Institute of Archaeology Iasi of the Romanian Academy, 6 Codrescu Street, 700479 Iasi, Romania. [3]Neaspec GmbH, Bunsenstrasse 5, 82152 Martinsried, Germany. [4]Department of Natural and Synthetic Polymers, "Gheorghe Asachi" Technical University of Iasi, 67 D. Mangeron Bld., 700050 Iasi, Romania. ✉email: olaruma@icmpp.ro

silsesquioxane, methacrylate and fluorine units. Within this context, the paper reports the first mention of a chemically active functional coating that operates *via* specific photochemical transformations at the coating-air interface, during accelerated weathering in an oxygen-filled chamber at room temperature, for the protection of ceramic artefacts against UV light and water. To our knowledge, no demonstration on the attainment of a UV-resistant protective coating for cultural heritage artefacts based on the photochemical transformation of silsesquioxanes into ladder-like structures upon UV light irradiation was previously reported. In addition, the paper reports the first investigation of the photo-degradation behavior of protective coatings through nano-FTIR technique.

RESULTS AND DISCUSSION

Structural characterization of PB72 and AMF

AMF polymer was obtained through hydrolysis and polycondensation of TMSPMA and TFPTMS in the presence of dodecylamine surfactant in order to obtain a crack-free film while drying[4]. The structure of PB72 and the complete synthesis reaction for AMF is presented in Fig. 1.

PB72 was selected as a reference commercial product for a comparative estimation of the coating performance of AMF since both compounds contain methacrylate units. The structure of PB72 and AMF was confirmed by nuclear magnetic resonance (NMR, Supplementary Fig. 1), Fourier-transform infrared (FTIR) and nano-FTIR spectroscopies. Figure 2 shows the FTIR spectra of PB72 and AMF before and after UV irradiation and the assignments of the absorption bands of PB72 and AMF are presented in Supplementary Information (description, Supplementary Table 1).

Apart from the main characteristic absorption bands, the presence of CH out-of-plane deformation vibration of >C = CH- group at 861 cm^{-1} (Fig. 2a) shows the existence of double bonds before UV irradiation of PB72 films. The presence of these groups can be attributed to the elimination of some ester units from methacrylate groups[16] and formation of C = C double bonds in the main chain during handling. The absorption bands that undergo noticeable changes during first ageing cycle are related to hydroxyl, CH stretching, carbonyl (C = O stretching belonging to γ-lactones[17,18]) and ester (C-O-C) functionalities. During the second ageing cycle, the OH peak intensity decreased indicating extensive photo-oxidation reactions of hydroxyl units and formation of oxidized products bearing C = O chromophores[19]. Furthermore, a progressive increase and broadening of the C = O stretching absorption bands of esters and γ-lactones (1735, 1720 and 1783 cm^{-1}), as well as the decrease of the absorption band from 1650 cm^{-1} that can be attributed to internal double bonds was registered.

For AMF (Fig. 2b), the main asymmetric Si-O-Si absorption bands illustrate the presence of both cage- (cages - 1128 cm^{-1}, poly-cages - 1173 cm^{-1}) and ladder-like structures (open-cages - 1070 cm^{-1}, cycles of low condensation degree - 1022 cm^{-1}). Other characteristic bands of AMF polymer are presented in Supplementary Information (detailed information, Supplementary Table 1). A decrease of the OH peak due to the photo-oxidation reaction of hydroxyl units and subsequent formation of oxidized products comprising C = O chromophores[19] was registered during the first ageing cycle. The minor loss of low molecular weight materials is evidenced by the decrease of the absorption bands from 2986 cm^{-1} and of most of the bands found in the fingerprint region (1400 - 700 cm^{-1}). The disappearance of the 1698 cm^{-1} absorption band (C = O units, hydrogen bonding and/or dipolar-type interaction) and the significant decrease of the C = O stretching band (1723 - 1738 cm^{-1} region) illustrates the formation of aldehydes and/or esters. Except Si-O-Si stretching bands, a minor decrease of all other bands in the fingerprint region was noticed during the second ageing cycle, indicating the loss of small amounts of low molecular weight compounds.

The exponential increase of PB72 carbonyl index (C.I. = $A_{1723\ cm^{-1}}/A_{755\ cm^{-1}}$, A - peak absorbances) from 2.34 to 2.62 and up to 5.01 during the first and second ageing cycles, respectively, illustrates the continuous formation of oxidation products bearing C = O chromophores mainly through chain scission. The small increase of C.I. during the first cycle suggests a competition between the development and cleavage of the crosslinked structures formed between the radically active C-O· sites connected to the photo-destruction of π bond from C = O group, while the strong increase of C.I. in the second stage illustrates the predominant cleavage through chain scission[19]. The steady decrease of AMF carbonyl index (C.I. = $A_{1723\ cm^{-1}}/A_{1269\ cm^{-1}}$) from 1.86 to 0.91 and up to 0.87, respectively, illustrates the photo-destruction of π bonds from C = O group, formation of C-O· radicals and crosslinked structures[19].

Nano-FTIR spectroscopy (Fig. 3) enabled a detailed spectroscopic analysis of polymer coating surfaces at 20 nm resolution scale. Nano-FTIR spectrum of PB72 (Fig. 3a) shows the presence of the stretching modes of PMA carbonyl and hydrogen bonded carbonyls at 1730 cm^{-1} and 1697 cm^{-1}, respectively. The presence of only PMA carbonyl at the surface may be explained by a preferential orientation of this group at the outer surface of the polymeric coating, while PEMA carbonyl is oriented toward the bulk. The driving force for the preferential orientation can be attributed to the stronger intermolecular hydrogen bonding between the PEMA carbonyl units and traces of water from acetone solvent due to the higher negative inductive effect and electron contribution of ethyl methacrylate units to carbonyl group[20]. Other characteristic bands of PB72 are presented in Supplementary Table 2.

During first ageing cycle, all absorption bands in the fingerprint region decreased and several carbonyl bands due to Fermi resonance of α, β-unsaturated γ-lactones (1773 and 1791 cm^{-1}) and of carboxylic acid dimers (1714 cm^{-1})[21] appeared in the carbonyl region. The formation of α,β-unsaturated γ-lactones was further confirmed by the presence of C = C double bond of lactone ring (1605 cm^{-1}), CO stretching (1203 cm^{-1}), C = C stretching vibrations of >C = CH- group from trisubstituted alkenes (1690 cm^{-1}) and >C = CH- in conjugation with C = O (1646 cm^{-1})[21]. The absorption bands from 1012 cm^{-1} (CH wagging), 1376 cm^{-1} (CH in plane deformation) and 1646 cm^{-1} (C = C stretching) indicate the formation of vinylene –CH = CH- moieties[21]. The same trend was observed during the second cycle.

Nano-FTIR spectrum of AMF (Fig. 3b) evidenced the presence of cage-like, open-cages and cycles of silsesquioxane units of low condensation degree at 1123 cm^{-1}, 1070 cm^{-1} and 1029 cm^{-1}, respectively. The hydrogen bonded carbonyls appeared at 1697 cm^{-1}, while the main carbonyl stretching vibration was shifted toward higher frequency (from 1723 to 1739 cm^{-1}) as compared to the corresponding FTIR spectrum, likely due to the preferential arrangement of the silsesquioxane structural units (directly linked to carbonyl groups) with the smallest crystallinity degree at the outermost surface layer[22]. The open-caged silsesquioxanes are characterized by the smallest crystallinity degree due to the presence of flexible structures[23]. Moreover, the nano-FTIR spectrum illustrated a smaller intensity (up to three times) of the carbonyl peak when normalized to the silsesquioxane main absorption bands. Presumably, in addition to CF_3 groups, the propyl groups from TMSPMA units are oriented away from the surface of AMF film, while the methylene units from the main chains are oriented in the plane of the surface characterized by a more close-packed structure[17]. From a thermodynamic point of view, the formation of an ordered and partially oriented local configuration of propyl and CF_3 groups at the surface is favoured by lower free energy. This local configuration partially covers and, to some extent, shields surface OC = O groups from UV irradiation.

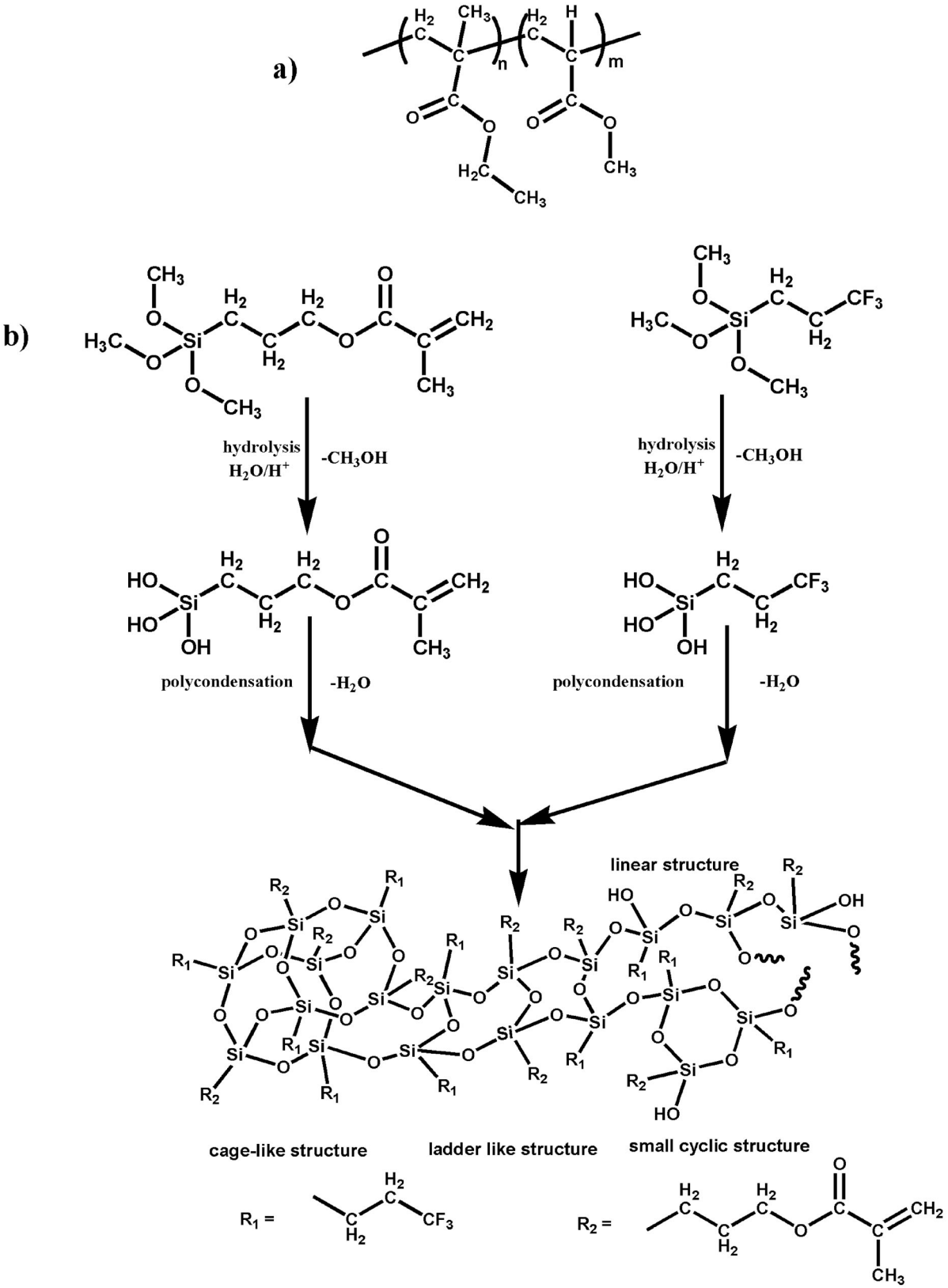

Fig. 1 The chemical structure of the investigated polymers. a PB72 and **b** AMF with the complete synthesis pathway.

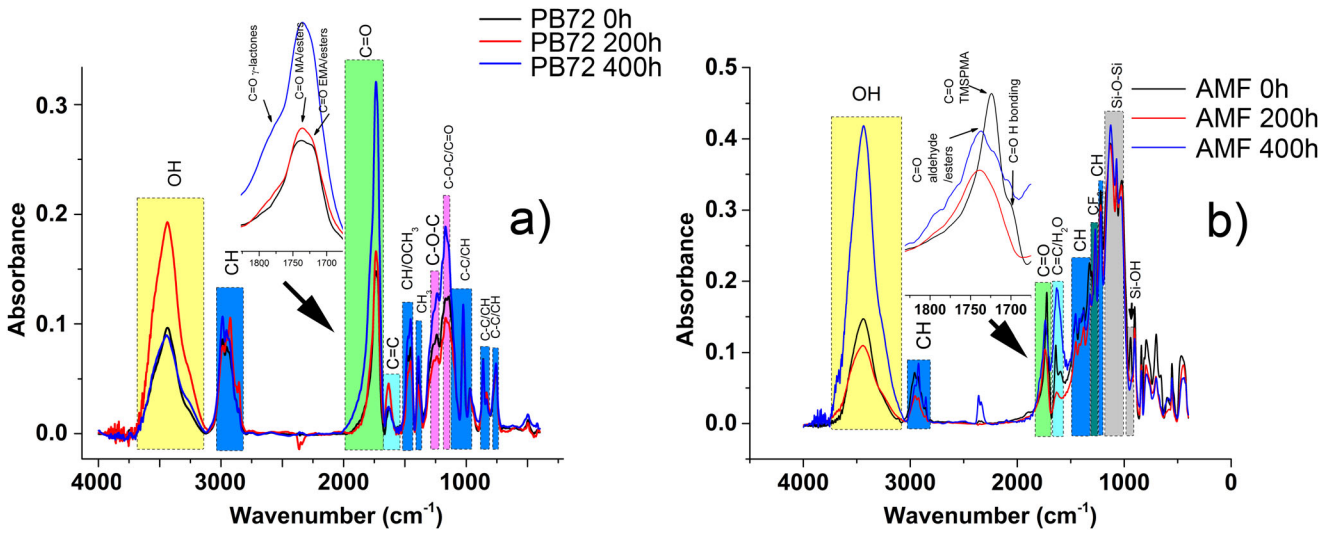

Fig. 2 FTIR spectra of the investigated polymers. a PB72 and **b** AMF before (——) and after (—— 200 h, —— 400 h) UV irradiation.

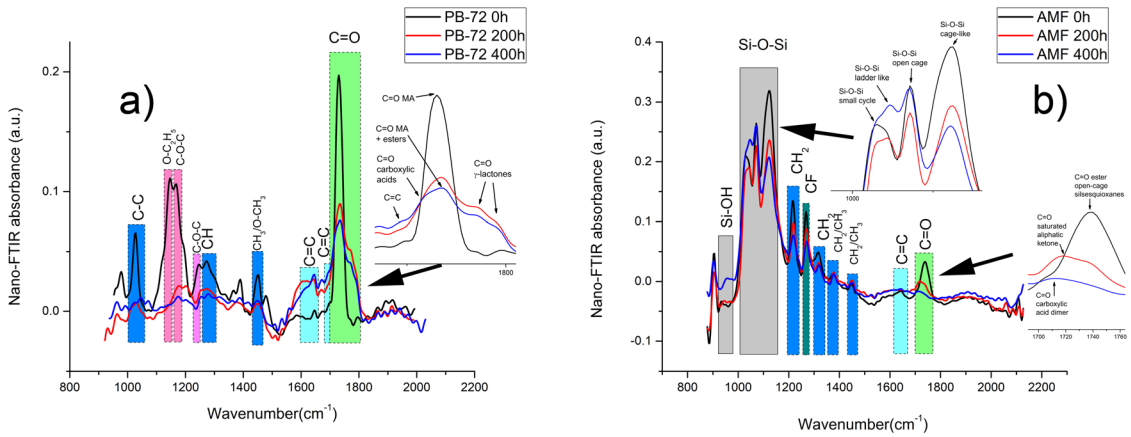

Fig. 3 Nano-FTIR spectra of the investigated polymers. a PB72 and **b** AMF before (——) and after UV irradiation (——200 h, ——400 h).

Other characteristic bands of AMF are presented in Supplementary Table 2.

A decrease of the Si-O-Si asymmetric stretching bands from 1124 cm^{-1} (cage-like), 1071 cm^{-1} (open-cages) and 1031 cm^{-1} (small cyclic structures), as well as the appearance at 1044 cm^{-1} of an absorption band that can be attributed to the Si-O-Si asymmetric stretching of ladder-like silsesquioxane units[24] was noticed during AMF first ageing cycle. The further growth of the intensity of Si-O-Si asymmetric stretching and its small shifting toward a higher wavelength (1047 cm^{-1}) during the second cycle can be correlated with a slight increase of the thickness of the ladder-like layer[25]. Figure 4 is presenting the evolution of the silsesquioxane structures with open cages into a ladder-like network.

In order to evidence the appearance of this particular type layer on the surface of aged AMF samples, SNOM images were acquired for both AMF samples subjected to ageing cycles at the wavelength of the ladder-like structures formed due to the action of the UV light (1044 cm^{-1}) (Supplementary Fig. 4). These images showed the formation of a layer with a more homogeneous structure and fewer defects on the surface of AMF sample exposed to prolonged irradiation as compared to the one irradiated for only 200 h. An increase of Si-O-Si asymmetric stretching bands from 1031 cm^{-1} (small cyclic structures) and from 1071 cm^{-1} (open cages) up to their initial intensity, as well as the decrease of the intensity of Si-O-Si asymmetric stretching band from 1121 cm^{-1} (cage-like) was registered during the second accelerated ageing cycle. As regards CH vibrations, the appearance of an absorption band (>C = CH-, CH in plane deformation vibration of a trisubstituted alkene) at 1348 cm^{-1} and its shift to 1351 cm^{-1} during the first and second ageing cycles, respectively, was noticed in the corresponding nano-FTIR spectra of AMF samples. Another important feature of the UV exposure was related to the decrease of the carbonyl band from 1739 cm^{-1} and to the appearance of other two additional bands located at 1718 (saturated aliphatic ketone) and 1712 cm^{-1} (carboxylic acid dimer). The loss of ester groups may be considered the main degradation process, as illustrated by the decrease of the intensity and area of the 1739 cm^{-1} main carbonyl stretching band.

Permeability measurements

Dynamic vapor sorption measurements (Supplementary Fig. 5, detailed information, Supplementary Information) evidenced the microporous nature of both protective coatings, being registered average pore sizes of 1.73 nm and 1.42 nm for PB72 and AMF, respectively. Since both PB72 and AMF are microporous, one may assume that these ones will allow the ceramic samples to "breathe", i.e., ceramics will remain permeable to water vapor

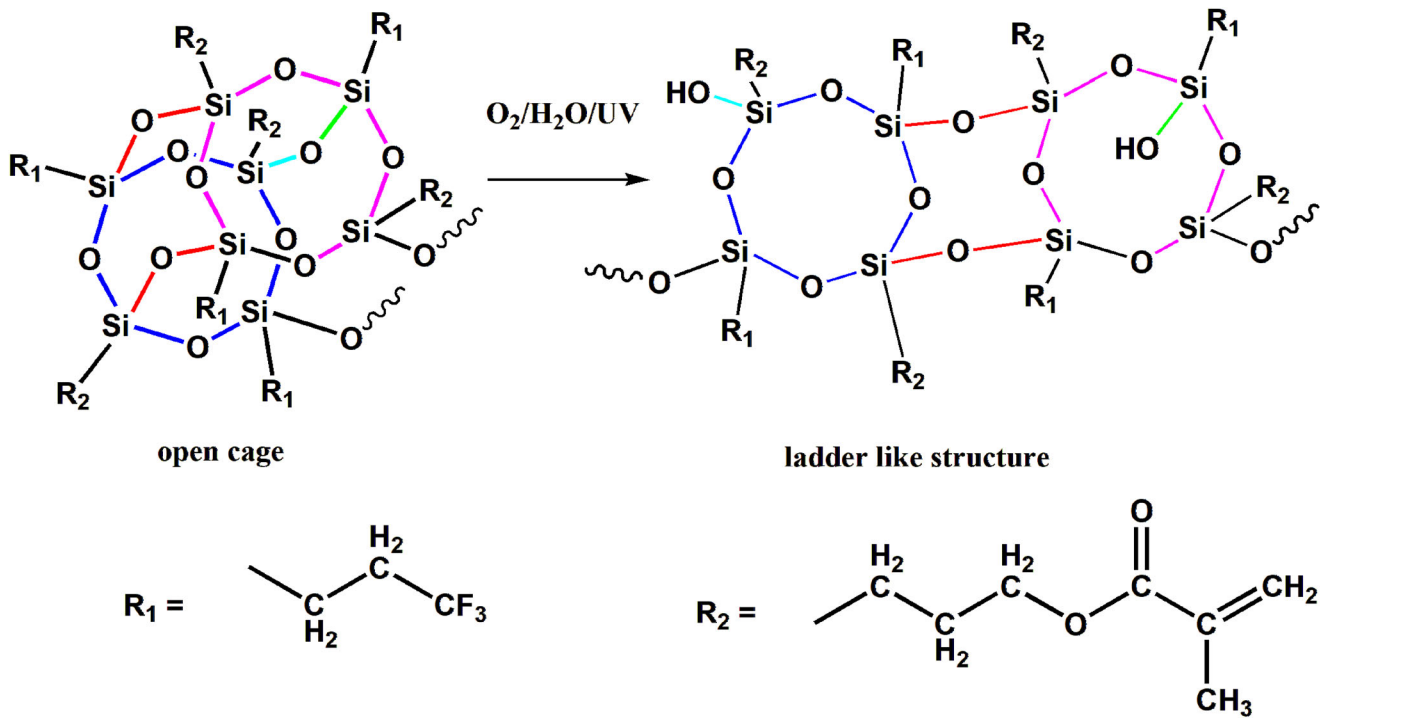

Fig. 4 Evolution of the silsesquioxanes with open cages into ladder-like structures.

thus avoiding the accumulation of moisture at the interface between the treated area and untreated ceramics.

Surface morphology of PB72 and AMF coatings before and after UV irradiation

The variation of the morphology of the thin films before and after ageing cycles was investigated through AFM technique. Figures 5 and 6 present two-dimensional (2D) and three-dimensional (3D) AFM images of AMF and PB72 coatings, respectively.

AFM measurements confirmed the extensive photodegradation of PB72 thin films during ageing cycles. During the first cycle, blisters that peeled off from the outermost surface layer of PB72 (Figs. 5b, 6b) as a consequence of the flaking and cracking process were observed. The complete cracking of the surface layer (Figs. 5c, 6c) that can easily allow for water and other degradation agents to deeply penetrate within the film substrate was noticed during the second cycle. As regards AMF coating, no evidence of cracks or blisters as a consequence of aging process was noticed. The round nano-scaled protrusions (microphase-separated domains, Figs. 5e, 6e) formed during the first cycle were found to coalesce, during the second stage, into hexagonal-like "islands" (approx. 23 nm height, 2 μm lateral dimensions), resembling the hexagonal shape of silsesquioxane clusters[26].

The morphologic investigations of the samples relied on SEM in the case of the ceramics (Fig. 7) because their rough surface makes analysis by AFM impossible and the thin films of PB72 showed signs of degradation when exposed to the SEM beam. The SEM analysis of sample 41 (example) shows that the PB72 polymer layer is much thicker (Fig. 7b), with local accumulations appearing depending on the area whereas for AMF the surface is evenly coated and the overall morphology of the ceramic does not change significantly (Fig. 7c). SEM images obtained after the second cycle show that AMF and PB72 have very different behaviors. For PB72 (Fig. 7d) the formation of micro-cracks is clearly observable and reflects, at a micro-scale, the cracking and flaking processes observed on the thin film samples deposited on glass plates. As regards AMF (Fig. 7e), no obvious differences between the initial samples and the ones exposed to UV ageing could be observed, in part due to the very thin layer of the polymeric coating. EDX measurements are presented in Supplementary Table 3 (detailed information, Supplementary Information).

Chromaticity investigation

The color changes of the two protective coatings upon UV irradiation were investigated on both glass and ceramic substrates. After the first ageing cycle, the PB72 coating showed increased ΔE^* and decreased ΔL^*, characteristic of polymeric chain scission due to photo-degradation. Also, the increase of Δb^* may be correlated with the formation of oxidative products during chain scission[19]. The increase in C = O moieties is compensated by the partial loss of carbonyl groups and formation of crosslinking structures, as evidenced by Δa^* decrease. The increase of both ΔL^* and ΔE^* during the second cycle indicates that the surface of PB72 has completely faded and larger cracks are present on the outer surface (in correlation with SEM images). Also, the decrease of Δb^* illustrates the degradation of the oxidative products.

As regards AMF coating, a decrease of ΔL^*, Δa^* and Δb^* parameters that can be associated with the reduction of C = O groups due to their involvement in the formation of subsequent crosslinking structures (C-O·)[19] was registered during the first ageing cycle. The decrease of ΔE^* (lower that the control value with around 16%) may indicate that AMF can be regarded as an anti-ageing polymer that succeeded to effectively absorb the UV light and limited the fade phenomenon. During the second cycle, the small increase of Δb^* and Δa^* decrease indicates that the small increase in C = O concentration is compensated by the partially loss of carbonyl groups and formation of crosslinking structures. The continuous decrease of ΔE^* (from 16% to around 23%) suggests that AMF exerts a better protective effect with increased irradiation time. The decrease of both ΔE^* and ΔL^* may suggest that only a slow degradation of AMF occurs, with different levels of photo-degradation between the outer and inner core.

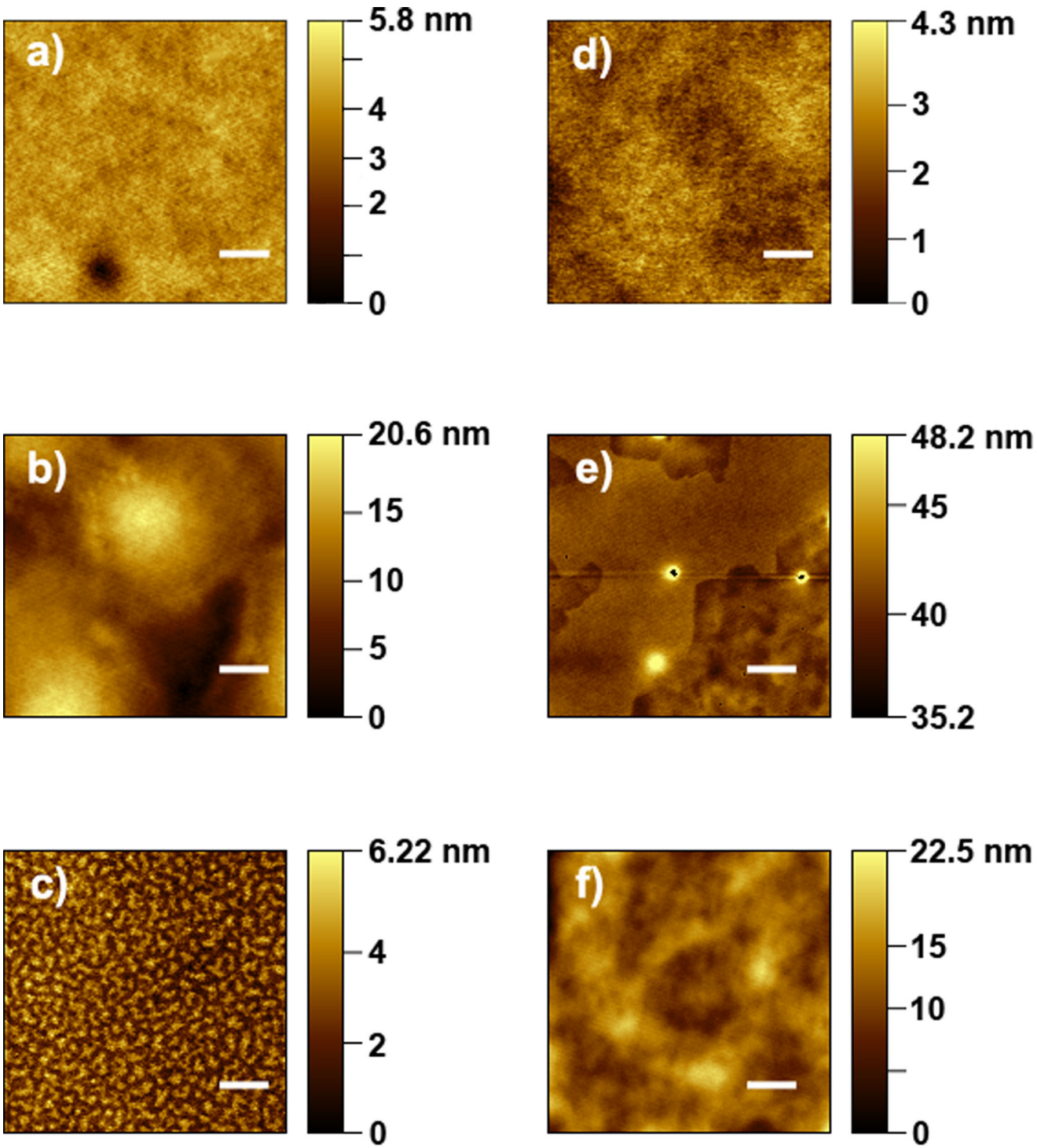

Fig. 5 2D AFM images (6 × 6 µm) of AMF and PB-72 thin film samples over the course of the accelerated ageing cycles. a 0, **b** 200 and **c** 400 h of UV irradiation of AMF samples and **d** 0, **e** 200 and **f** 400 h of UV irradiation of PB-72 samples. Scale bar in all images is of 1 µm.

As regards the polymeric coatings of the ceramic substrates, the chromaticity investigation yielded a variation of the color parameters which does not follow the same behavior as reported for the same polymeric coating on glass substrate and even between the different types of ceramics. The disparity between these results can be ascribed to the presence of coarse inclusions and tempers of different colors inside and on the surface of the ceramic sherds[27]. Even in this situation, the AMF coating yielded smaller ΔE* variation as compared to PB72 one. The data regarding the polymeric coatings on ceramic substrates were submitted to further statistical analyses in order to identify whether significant patterns of color variation exist. Following exploratory data analysis (Supplementary Fig. 5, Supplementary Tables 4, 5 and 6) and contrasting two models of linear regression (detailed description, Supplementary Figs. 6 and 7, Supplementary Table 7, Supplementary Information) suitable for

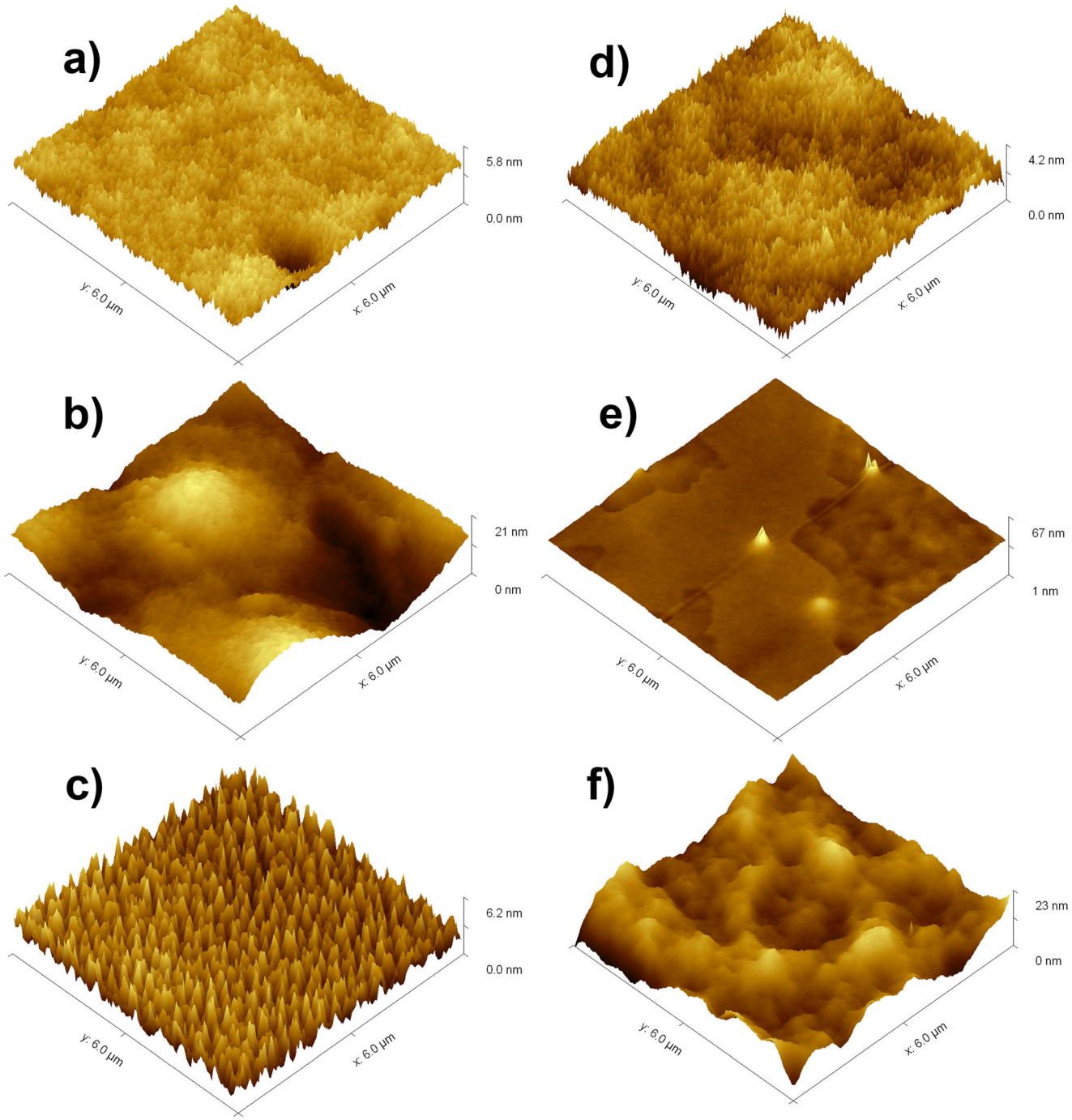

Fig. 6 3D AFM images (6 × 6 µm) of AMF and PB-72 thin film samples over the course of the accelerated ageing cycles. a 0, **b** 200 and **c** 400 h of UV irradiation of AMF samples and **d** 0, **e** 200 and **f** 400 h of UV irradiation of PB-72 samples.

longitudinal data[28], the analysis was run using a linear mixed effect modelling (Supplementary Table 8). This approach allowed the sample variable to be nested within the treatment factor, which is compared against the value (color distance) variable. In order to evidence the differences, we have conducted a Tukey Contrasts multiple comparisons of means with the results summarized in Supplementary Information (Supplementary Table 9, Supplementary Fig. 8). The results allow us to conclude that AMF treatment, when compared to the PB72 coating, is characterized by greater stability and provides not only lower color deviation from the original, but also better color conservation after UV aging.

Contact angle measurements

The contact angle measurements were performed on both glass and ceramic substrates. While a drastic decrease of the contact angles was registered for PB72 (from 90.90 up to 18.3), only a small decrease of this parameter (from 98.63 up to 82.13) was evidenced for AMF on glass substrate after both ageing cycles. The polymeric coatings applied onto the ceramic substrates yielded different contact angle values as compared with the ones performed on glass substrates (detailed description, Supplementary Table 10, Supplementary Information). All measurements of AMF coatings of the ceramic sherds exceeded the values of the

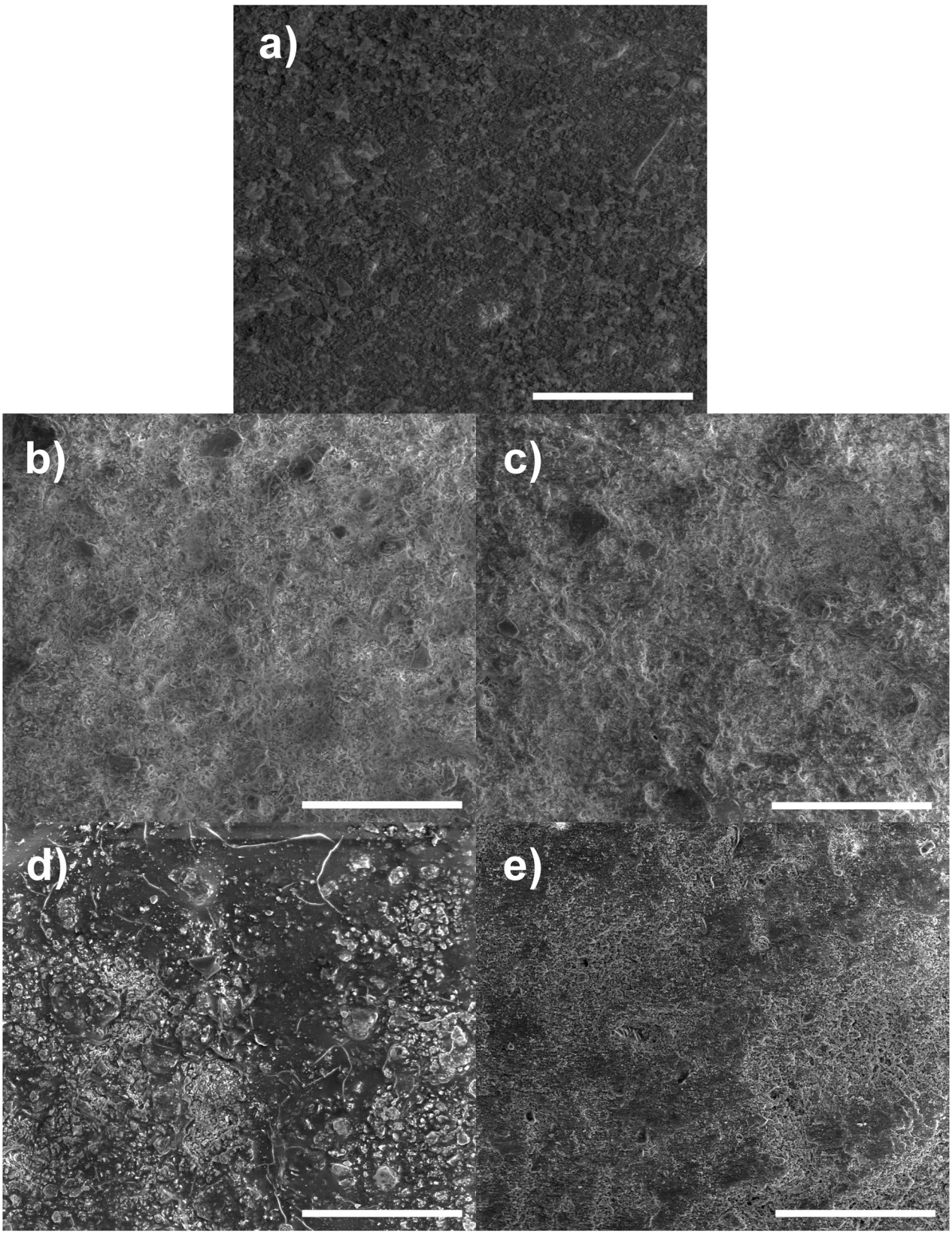

Fig. 7 SEM morphology of sample 41. a uncoated, coated with **b** PB72 and **c** AMF, coated with **d** PB72 and **e** AMF and exposed to 400 h UV irradiation. Scale bar in all images is of 200 µm.

coatings performed on the glass substrate, i.e., from 109. 9 (average value of sample 55) to 123.8 (average value of sample 44), while PB72 coating yielded both smaller, i.e., 83.1 (the smallest average value for sample 40) and higher contact angle values, i.e., 115.5 (the highest average value for sample 55). This behavior can be connected with the different nature of the ceramic substrates, as well as to their high inhomogeneity and roughness[27]. Regardless of the initial value of PB72 coating, a drastic decrease of the contact angle value was registered for all ceramic samples after 200 h of UV irradiation, being recorded values between 15.53 and 34.00 for samples 41 and 42, respectively. The continuous decrease of PB72 contact angle values can be connected with the appearance of cracks on the outer layers and their enlargement that allow water to easily penetrate inside the ceramic sherds. As regards AMF coatings, with only three exceptions, i.e., the same contact angle value for sample 44 and two smaller values for samples 57 and 59, all wettability measurements evidenced an increase between 6–10% (up to 126.60 for sample 42) of the corresponding contact angle values as compared with the initial ones that can be ascribed to the crosslinking of methacrylate units and formation of hydrophobic -CH_2-CH_2- units. Following exploratory data analysis (Supplementary Figs. 9 and 10, Supplementary Table 11) and contrasting two models of linear regression suitable for longitudinal data (Supplementary Figs. 11 and 12, Supplementary Table 12), we have run our analysis using a linear mixed effect modelling (Supplementary Table 13), allowing the sample variable to be nested within the factor representing the interaction between treatment and aging time, which is compared against the variable value (values of contact angle). In order to synthesize the differences, we have conducted a Tukey Contrasts multiple comparisons of means with the results summarized in Supplementary Information (Supplementary Fig. 13, Supplementary Table 14). The results allow us to conclude that AMF treatment presents higher values and better endurance during aging, as opposed to the lower values and high variability of PB72 treatment.

Photobehavior of PB72 and AMF coatings during accelerated ageing cycles

During the first ageing cycle, the photoinduced degradation of PB72 films involved the main chain scission, process followed by the macroradical disproportionation and subsequent development of four types of C = C bonds belonging to α, β-unsaturated γ-lactones, vinylenes, α, β-unsaturated esters and trisubstituted alkenes, as well as carboxylic acid dimers. After the second cycle, an extensive chain scission of the main chain occurred and the initial degradative pathway continued with the degradation of the oxidative products. With the exception of α, β-unsaturated γ-lactones, the degradation pathway of PB72 components (Fig. 8) is following the same mechanism as the one proposed by Favaro et al.[29].

The photo-oxidative pathway of PMA involved the formation of vinylene and α, β-unsaturated esters groups (Fig. 8a) and subsequent development of α, β-unsaturated γ-lactones (only at PMA level due to its preferential orientation at the outer surface) by either the extraction of the hydrogen atoms linked to the tertiary carbons from methacrylate groups or from the oxidation in the same position and cyclization. As regards PEMA, the macroradical disproportionation yielded the appearance of α, β-unsaturated esters and trisubstituted alkenes (Fig. 8b). The carboxylic acid groups could appear due to the oxidation of the molecules comprising unsaturated C = C bonds with ozone (ozonolysis, Fig. 9). The presence of only carboxylic acid groups among the photo-oxidation products is illustrating that ozonolysis was performed only at –CH = CH– bonds (R_1 or R_3 = H).

A significant lower level of carbonyl groups, a delayed interchain hydrogen abstraction and subsequent oxidation of the main polymeric chain were registered for AMF coating, the main degradation effect being rather related with the crosslinking reaction than with the scission process. Presumably, a reaction between the oxygen molecules with the radicals formed upon the extraction of a secondary hydrogen atom from the structural units occurred during UV irradiation, followed by β-scission and appearance of α,β-unsaturated esters and trisubstituted alkenes (Fig. 10). The ozonolysis reaction of the C = C bond yielded the formation of ketone and carboxylic acid groups (Fig. 9).

Under UV irradiation, the chemically active coating comprising silsesquioxane units yielded, *via* specific photochemical transformations at the coating-air interface, the appearance of a ladder-like silsesquioxane layer acting as a UV protective barrier against photo-oxidative degradation. The binding energy of Si-O bonds is of 466 kJ/mol, therefore only the UV light from 253.7 nm can induce the photocleavage of Si-O-Si bonds into Si, O and O_2 species that mutually react to form ladder-like structures and silanol units[30]. Although the energy dose (39 mW/cm^2 for 400 h) was much higher than the one necessary for the complete conversion of all silsesquioxane units into a SiO_2-like network (ca. 30 J/cm^2)[31], most of the silsesquioxanes initially present in the polymer structure were preserved and the direct cleavage of Si-O bonds represented only a minor process of the UV irradiation. Due to its higher color stability (minimum color variation)[32] and the active role of free OH groups belonging to open-caged silsesquioxanes present at the outermost surface layer in the stabilization process (behavior similar to UV filters)[33], AMF can be regarded as an anti-ageing polymer that succeeded to effectively absorb the UV light and limited the fade phenomenon[32]. Apart from conferring chemical inertness, corrosion and wear resistance, low gas permeation and high transparency[34], the formation of ladder-like silsesquioxane structures by means of photochemical transformations has attractive features in terms of low cost, non-toxicity and eco-friendliness. In addition, the migration and local reorganization of fluoroalkyl and silsesquioxane units at the outermost layer and formation of microphase-segregated domains were found to induce a good water repellency and increased the overall resistance of AMF toward UV ageing.

The information provided by nano-FTIR technique, i.e., preferential orientation of specific functional groups (PMA and open-caged silsesquioxanes), formation of α, β-unsaturated γ-lactones as photo-degradation products onto the surface of aged PB72 and appearance of a ladder-like silsesquioxane layer *via* specific photochemical transformations at the coating-air interface had a significant role in determining the photodegradation mechanism of both PB72 and AMF protective coatings. The photo-degradation behavior of both compounds was mainly found to depend on the structure and properties at the polymer/air interfaces, as well as to the preferential orientation of specific functional groups at the outermost layer. While in PB72 the degradation process (influenced by the preferential orientation of PMA component at the outer layer) mostly occurred through an extensive chain scission of the main chain, the main degradation effect in case of AMF was rather related with the crosslinking of the long ester chains than with the scission process. The better protective behavior of AMF was ascribed to a synergetic effect of silsesquioxanes (ladder-like and open-caged structures) and fluorine that exerted a beneficial role and protected the polymeric chain against UV-induced photodegradation. The good hydrophobicity (even after exposure to prolonged UV irradiation), microporous nature, and anti-ageing features recommend AMF for the protection of ceramic artefacts against UV radiation.

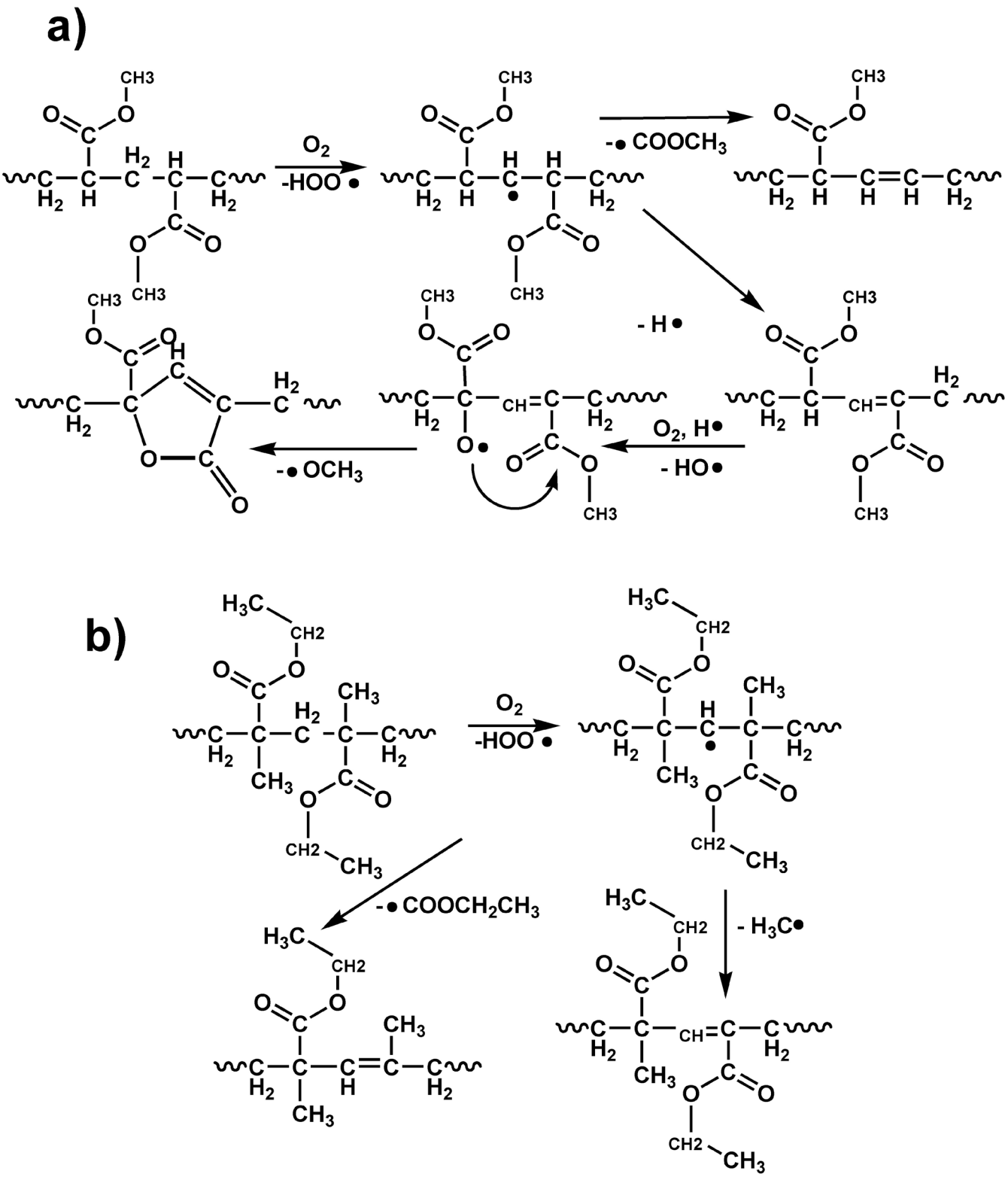

Fig. 8 Photo-oxidative degradation pathway of PB-72 structural units. a PMA and **b** PEMA components.

METHODS

Synthesis of AMF polymer

16,865 mmol (4 ml) 3-(trimethoxysilyl)propyl methacrylate (TMSPMA, Sigma Aldrich) and 16,865 mmol (3,22 ml) (3,3,3-trifluoropropyl) trimethoxysilane (3FPTMS, Sigma Aldrich), 13 ml isopropyl alcohol (Chemical Company) and 4 ml distilled water were added to a round bottom flask. A solution of 10 ml isopropyl alcohol and 4 drops of hydrochloric acid 33% (Chemical Company) was added until a pH of 5 was reached. 0.050595 mmol dodecylamine surfactant was added ensuring a molar ratio of 1 TMSPMA: 1 FPTMS: 0.003 dodecylamine. The hydrolysis and polycondensation reaction occurred at 40 °C and with mechanical stirring for 2 weeks.

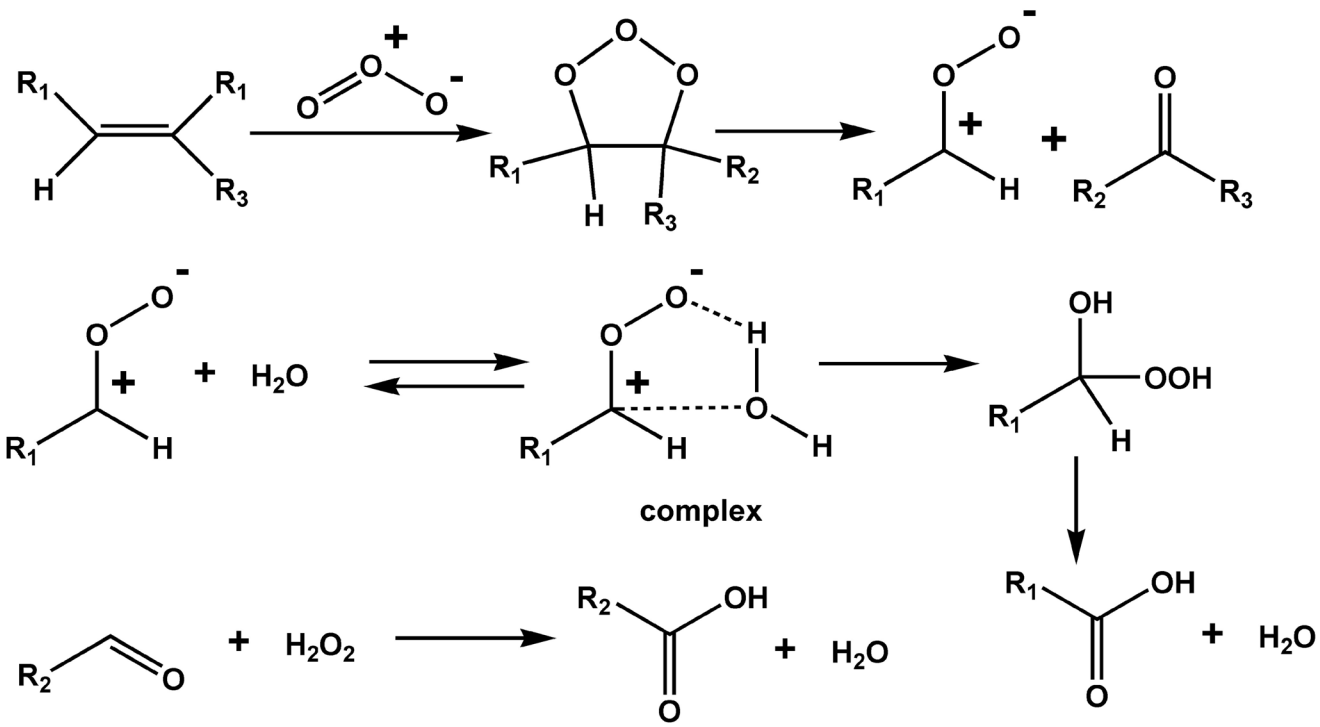

Fig. 9 Ozonolysis reaction of C = C bonds.

Application of conservation treatments

PB72 and AMF were applied on 9 samples of Neolithic Cucuteni pottery from Hoisesti—la pod archeological site, 3 each of coarse (samples 40, 66, 73), intermediate (samples 41, 42, 44) and fine ceramics (samples 55, 57, 59) as determined by optical microscopy[27]. After cleaning, the samples were dried in an oven at 80 °C for 48 hours and 9 pieces of each sample (~1 by 1 cm square) were cut from them. 3 were used for the application of PB72, 3 for AMF and 3 were kept as control. Polymers were applied by immersing the samples in 10% solutions of PB72/acetone or AMF/isopropyl alcohol for 6 min. PB72 and AMF were also deposited on 3 glass plates in the form of thin films.

Accelerated weathering

Accelerated weathering was performed in a laboratory chamber (Angellantoni Ind.) with all samples kept in identical conditions. Weathering cycles involved 200 h of exposure to artificial light of a mercury lamp ($\lambda = 200–700$ nm, incident light intensity 39 mW/cm^2) at a temperature of 30 °C and 60% humidity. In these conditions, the UV light whose wavelength is smaller than 242.4 nm is splitting the oxygen molecules into atomic oxygen and ozone. All ceramic samples (uncoated and coated) underwent two weathering cycles. In the case of thin films, one sample was kept as reference, one underwent an ageing cycle and another was exposed to two ageing cycles. After each cycle, color and contact angle measurements were carried out.

Experimental procedure

NMR analyses were performed with Bruker Avance NEO 400 MHz spectrometer, 5 mm direct detection, four nuclei probe (H, C, Si, F), standard pulse sequences and TopSpin 4.0.5 software. FTIR spectra were recorded with Bruker Vertex 70, 64 scans at room temperature using the KBr pellet technique and Opus 6.5 FTIR software. nano-FTIR measurements were performed on a neaSNOM system from neaspec, GmbH. Nano-FTIR spectra were collected in 3 random points on the surface of each sample (Supplementary Figs. 14 and 15) and the resulting average spectrum was used for interpretation. AFM measurements were performed in phase contrast tapping mode, using a scanning probe microscope Solver PRO-M with NSG10 cantilever (NTMDT) and Nova v.1.26.0.1443 software. SEM images were acquired using a Quanta 200 scanning probe microscope. Cromaticity investigations were performed on both glass and ceramic substrates with a portable MiniScan EZ 4500 L Spectrophotometer (Hunter Associates Laboratory) and 9 measurements in random points on the surface were acquired for the thin film samples and 6 for the ceramic samples, due to their small size. The measurements were presented in the L^*, a^*, b^* coordinates of CIE LAB system. Color change (ΔE^*) was calculated as $\Delta E^* = [(\Delta L^*)^2 + (\Delta a^*)^2 + (\Delta b^*)^2]^{1/2}$, where ΔL^* - difference in lightness, Δa^* - red green color difference, and Δb^* - blue yellow color difference. Static contact angle measurements were performed at room temperature with CAM101 (KSV Instruments) automatic instrument containing a liquid dispenser, drop-shape analysis software, a video camera and double distilled water solvent. Three various surface regions were analyzed in order to obtain a statistical result. Water vapors sorption capacity (25 °C, 0–90% relative humidity range) was determined by using a fully automated gravimetric analyzer IGAsorp, Hiden Analytical[17].

Water vapors sorption capacity of the samples at 25 °C and 0–90% relative humidity range (RH) was determined by using a fully automated gravimetric analyzer IGAsorp from Hiden Analytical, Warrington (UK). The drying of the samples before sorption measurements was carried out at 25 °C in flowing nitrogen (250 mL/min) until the weight of the sample was in equilibrium at RH < 1%. The sorption isotherms were modeled based on the following BET equation:

$$W = \frac{W_m \cdot C \cdot \mathrm{RH}}{(1 - \mathrm{RH}) \cdot (1 - \mathrm{RH} + C \cdot \mathrm{RH})} \quad (1)$$

where: W—weight of sorbed water, W_m—weight of water forming a monolayer, C—sorption constant and RH - relative humidity.

Specific surface area was calculated from BET equation. The relationship between the liquid volume V_{liq} and the percentage

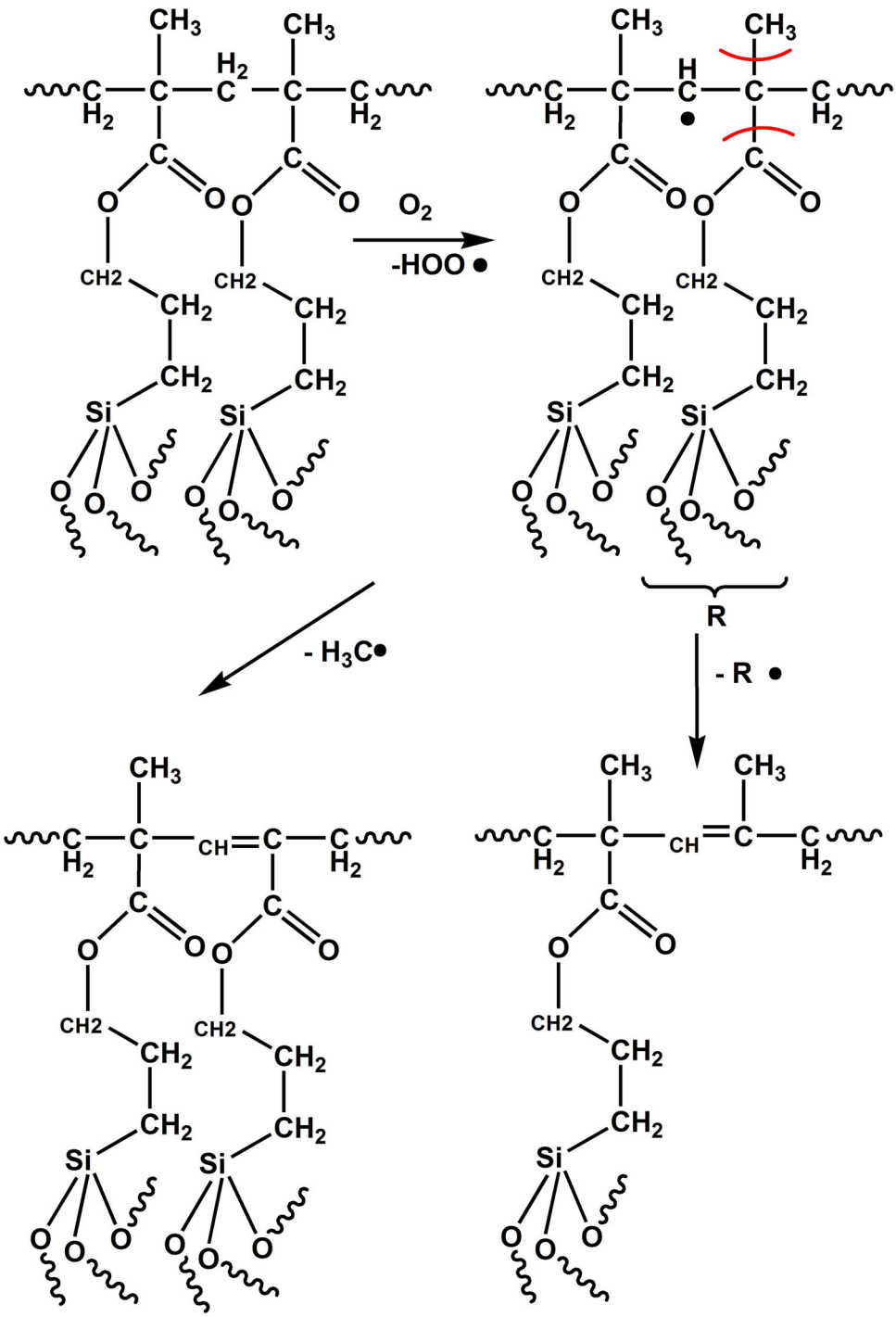

Fig. 10 Photo-oxidative degradation pathway of AMF.

uptake n, is evidenced in the following equation:

$$V_{liq} = \frac{n}{100 * \rho_a} \quad (2)$$

where: V_{liq} is the liquid volume, n is the percentage uptake and ρ_a is the adsorbed phase density. The average pore size was calculated from the pore volume assuming a cylindrical pore geometry:

$$r_{pm} = \frac{2 \cdot V_{liq}}{A} = \frac{2 \cdot n}{100 \cdot \rho_a \cdot A} \quad (3)$$

where: r_{pm} is the average pore size, V_{liq} is the liquid volume and A is the BET surface area.

The statistical analysis was performed in the R environment and language, overlaid by the integrated development environment of RStudio (Supplementary Information).

DATA AVAILABILITY

The data that support the finding of this study are available at https://doi.org/10.6084/m9.figshare.21443829.v3.

Received: 27 October 2022; Accepted: 15 March 2023;
Published online: 30 March 2023

REFERENCES

1. Constancio, C. et al. Studies on polymeric conservation treatments of ceramic tiles with Paraloid B-72 and two alkoxysilanes. *J. Appl. Polym. Sci.* **116**, 2833–2839 (2010).
2. Zhao, J. et al. TEOS/PDMS-OH hybrid material for the consolidation of damaged pottery. *Herit. Sci.* **1**, 1–10 (2013).
3. Botteghi, C. et al. Polyfluoroalkylmethacrylates as materials for the protection of stones. *Sci. Technol. Cult. Herit.* **1**, 111–122 (1992).
4. Simionescu, B., Olaru, M., Aflori, M., Buruiana, E. C. & Cotofana, C. Silsesquioxane-based hybrid nanocomposites of polymethacrylate type with self-assembling properties. *Solid State Phenom.* **151**, 17–23 (2009).
5. Simionescu, B. & Olaru, M. Assessment of siloxane-based polymeric matrices as water repellent coatings for stone monuments. *Eur. J. Sci. Theol.* **5**, 59–67 (2009).
6. Olaru, M., Aflori, M., Simionescu, B., Doroftei, F. & Stratulat, L. Effect of SO_2 dry deposition on porous dolomitic limestones. *Materials (Basel)* **3**, 216–231 (2010).
7. Simionescu, A. B. *Durability of Monumental Stones Treated With Siloxane-Based Water Repellents* https://doi.org/10.6092/UNIBO/AMSDOTTORATO/2268 (2009).
8. Chiantore, O., Lazzari, M., Aglietto, M., Castelvetro, V. & Ciardelli, F. Photochemical stability of partially fluorinated acrylic protective coatings I. Poly(2,2,2-trifluoroethyl methacrylate) and poly(1H,1H,2H,2H-perfluorodecyl methacrylate-co-2-ethylhexyl methacrylate)s. *Polym. Degrad. Stab.* **67**, 461–467 (2000).
9. Höpken, J. & Möller, M. Low-surface-energy polystyrene. *Macromolecules* **25**, 1461–1467 (1992).
10. Banerjee Poly(fluoroacrylate)s with tunable surface hydrophobicity *via* radical copolymerization of 2,2,2-trifluoroethyl α-fluoroacrylate and 2-(trifluoromethyl) acrylic acid. *Polym. Chem.* **8**, 1978–1988 (2017).
11. Liu, C. et al. Light stabilizers added to the shell of *co*-extruded wood/high-density polyethylene composites to improve mechanical and anti-UV ageing properties. *R. Soc. Open Sci.* **5**, 1–11 (2018).
12. Ahajji, A., Irmouli, Y., George, B. & Charrier, B. & Merlin, A. Inorganic UV absorbers for the photostabilisation of wood-clearcoating systems: comparison with organic UV absorbers. *Appl Surf. Sci.* **253**, 3737–3745 (2007).
13. Mahltig, B. et al. Optimized UV protecting coatings by combination of organic and inorganic UV absorbers. *Thin Solid Films* **485**, 108–114 (2005).
14. Olson, E. et al. Thin biobased transparent UV-blocking coating enabled by nanoparticle self-assembly. *ACS Appl. Mater. Interfaces* **11**, 24552–24559 (2019).
15. Verkholantsev, V. V. Chemically active coatings. *Eur. Coat. J.* **10**, 32–37 (2003).
16. Melo, M. J., Bracci, S., Camaiti, M., Chiantore, O. & Piacenti, F. Photodegradation of acrylic resins used in the conservation of stone. *Polym. Degrad. Stab.* **66**, 23–30 (1999).
17. Zhang, Y. et al. Influence of the linkage type between the polymer backbone and side groups on the surface segregation of methyl groups during film formation. *Soft Matter* **11**, 9168–9178 (2015).
18. Chiantore, O., Trossarelli, L. & Lazzari, M. Photooxidative degradation of acrylic and methacrylic polymers. *Polymer* **41**, 1657–1668 (2000).
19. Shanti, R. et al. Degradation of ultra-high molecular weight poly(methyl methacrylate-co-butyl acrylate-co-acrylic acid) under ultra violet irradiation. *RSC Adv.* **7**, 112–120 (2017).
20. Oswal, S. L., Patel, B. M., Patel, A. M. & Ghael, N. Y. Densities, speeds of sound, isentropic compressibilities, and refractive indices of binary mixtures of methyl methacrylate with hydrocarbons, haloalkanes and alkyl amines. *Fluid Phase Equilib.* **206**, 313–329 (2003).
21. Socrates, G. *Infrared and Raman Characteristic Group Frequencies: Tables and Charts* 3rd edn (John Wiley & Sons Ltd, 2001).
22. Cole, K. C., Guevremont, J., Ajji, A. & Dumoulin, M. M. Characterization of surface orientation in poly(ethylene terephthalate) by Front-Surface Reflection Infrared Spectroscopy. *Appl. Spectrosc.* **48**, 1513–1521 (1994).
23. Katoh, R., Imoto, H. & Naka, K. One-pot strategy for synthesis of open-cage silsesquioxane monomers. *Polym. Chem.* **10**, 2223–2229 (2019).
24. Koželj, M. & Orel, B. Synthesis of polyhedral phenylsilsesquioxanes with KF as the source of fluoride ion. *Dalton Trans.* **37**, 5072–5075 (2008).
25. Boyd, I. W. & Wilson, J. I. B. A study of thin silicon dioxide films using infrared absorption techniques. *J. Appl. Phys.* **53**, 4166–4172 (1982).
26. Kim, P., Zheng, Y. & Agnihotri, S. Adsorption equilibrium and kinetics of water vapor in carbon nanotubes and its comparison with activated carbon. *Ind. Eng. Chem. Res.* **47**, 3170–3178 (2008).
27. Oancea, A. V. et al. M. Multi-analytical characterization of Cucuteni pottery. *J. Eur. Ceram. Soc.* **37**, 5079–5098 (2017).
28. Fox, J. *Applied Regression Analysis and Generalized Linear Models* 2nd edn (Sage Publications Inc., 2008).
29. Favaro, M. et al. Evaluation of polymers for conservation treatments of outdoor exposed stone monuments. Part I: Photo-oxidative weathering. *Polym. Degrad. Stab.* **91**, 3083–3096 (2006).
30. Kim, Y., Zhao, F., Mitsuishi, M., Watanabe, A. & Miyashita, T. Photoinduced high-quality ultrathin SiO_2 film from hybrid nanosheet at room temperature. *J. Am. Chem. Soc.* **130**, 11848–11849 (2008).
31. Yamamoto, S., Sonobe, K., Miyashita, T. & Mitsuishi, M. Flexible SiO_2 nanofilms assembled on poly(ethylene terephthalate) substrates through a room temperature fabrication process for nanoscale integration. *J. Mater. Chem. C.* **3**, 1286–1293 (2015).
32. Chang, S.-T. & Chou, P.-L. Photo-discoloration of UV-curable acrylic coatings and the underlying wood. *Poly. Degrad. Stab.* **63**, 435–439 (1999).
33. Dintcheva, N. T. Z. et al. UV-stabilisation of polystyrene-based nanocomposites provided by polyhedral oligomeric silsesquioxanes (POSS). *Polym. Degrad. Stab.* **97**, 2313–2322 (2012).
34. Amendola, E., Cammarano, A. & Acierno, D. In *es* 23–40 (InTech, London, 2011).

ACKNOWLEDGEMENTS

The financial support of European Social Fund for Regional Development, Competitiveness Operational Programme Axis 1—Project "Petru Poni Institute of Macromolecular Chemistry - Interdisciplinary Pol for Smart Specialization through Research and Innovation and Technology Transfer in Bio(nano)polymeric Materials and (Eco)Technology", InoMatPol (ID P_36_570, Contract 142/10.10.2016, cod MySMIS: 107464) is gratefully acknowledged.

AUTHOR CONTRIBUTIONS

The manuscript was written through contributions of all authors. All authors have revised and have given approval for the final version of the manuscript. A.V.O. had a significant contribution to the synthesis of the AMF polymer and on the interpretation of SEM/EDX and AFM data agreeing for all aspects to ensure that all questions related to the accuracy of the work were properly investigated and resolved, G.B. performed the statistical analyses, A.C. provided the acquirement of nano-FTIR spectra and SNOM images agreeing with the assignments of the absorption bands, I.S. performed the ageing tests agreeing with the photo-degradation behavior of the analyzed compounds, A.N. made the acquisition of NMR spectra and had a significant contribution to their interpretation, M.D. made the acquisition of FTIR spectra and had a significant contribution to their interpretation, C.C. assured the technical support, discussed the content of the manuscript and aided in the design of the work, B.C.S. provided the input for the conception and organization of the work, while M.O. wrote the manuscript performing analysis and data interpretation.

COMPETING INTERESTS

The authors declare no competing interests.

ADDITIONAL INFORMATION

Supplementary information The online version contains supplementary material available at https://doi.org/10.1038/s41529-023-00343-8.

Correspondence and requests for materials should be addressed to Mihaela Olaru.

Reprints and permission information is available at http://www.nature.com/reprints

Publisher's note Springer Nature remains neutral with regard to jurisdictional claims in published maps and institutional affiliations.